CHEMISTRY OF MATERIALS
Cite This: Chem. Mater. 2018, 30, 7840−7851
Article
pubs.acs.org/cm

Conjugated Oligomers with Stable Radical Substituents: Synthesis, Single Crystal Structures, Electronic Structure, and Excited State Dynamics

Yiming Huang,[†] Zihao Xu,[§] Shijian Jin,[§] Chenyang Li,[§,∥] Kurt Warncke,[⊥] Francesco A. Evangelista,*[,§,∥] Tianquan Lian,*[,§] and Eilaf Egap*[,†,‡]

[†]Department of Materials Science and NanoEngineering and [‡]Department of Chemical and Biomolecular Engineering, Rice University, Houston, Texas 77005, United States

[§]Department of Chemistry, [∥]Cherry L. Emerson Center for Scientific Computation, and [⊥]Department of Physics, Emory University, Atlanta, Georgia 30322, United States

Supporting Information

ABSTRACT: Understanding and controlling spin dynamics in organic semiconductors is of significant technological interest. We present a comprehensive joint experimental and computational study elucidating excited-state dynamics and kinetics of oligothiophenes covalently linked to two radicals. The synthesis, steady-state, and ultrafast photophysics, magnetic properties, computational modeling, and single crystal X-ray diffraction of a series of oligothiophenes with appended nitronyl nitroxide (NN) diradicals (**RAx** and **RBx**) are presented. We show that incorporation of the diradicals results in an intriguing molecular packing that is reminiscent of organic cages, unusual excited-state dynamics, and interesting photophysical and magnetic properties. We find an increase in the distance and dihedral angle between the diradical rings and the oligothiophene core result in weak antiferromagnetic interactions. Single crystal X-ray diffraction and computational modeling suggest that efficient conjugation along the backbone leads to an efficient spin-polarization transfer. Insertion of *p*-phenylene linkers that separate the oligothiophene core from the NN radical component by an average of only 4.3 Å results in a decrease in orbital overlap between the chromophore and singly occupied molecular orbital of the two NN radicals and a weak spin polarization along the thiophene core. Computations also predict a biradical ground state with a small singlet−triplet energy gap (ΔE_{ST}) of 0.6 kcal/mol or less, where the triplet lies above the singlet, suggesting that in some of these molecules both the singlet and triplet states are thermally populated. Together, the steady-state optical absorption, computational study, and ultrafast transient absorption suggest enhanced internal conversion is the dominant pathway for rapid decay in **RAx** and **RBx** diradical series due to two major factors: (i) incorporation of the radicals results in new low-lying singlet and triplet states (S_1/T_1) that act as "trap states"; and (ii) generation of multiple singlet and triplet states that are essentially degenerate in energy. Since incorporation of NN diradicals leads to more than 20 low-lying near degenerate singlet, triplet and quintet states, both intersystem crossing and internal conversion become viable decay mechanisms for the decay of the S_n and T_n states back to the S_0 and T_0. These results establish and correlate structural and electronic parameters that impact spin coupling, spin delocalization, and determine general trends in predicting energy levels of excited states.

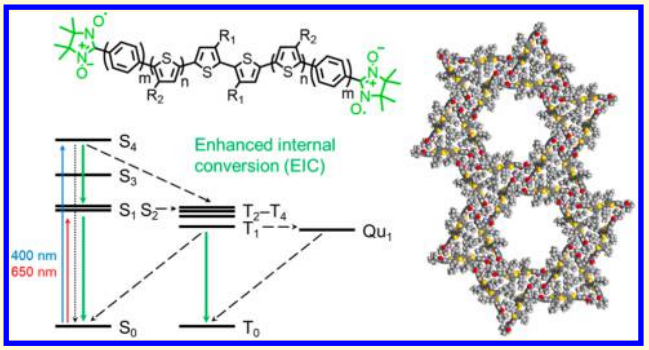

INTRODUCTION

Controlling electron spin dynamics is of significant fundamental and technological interests in organic semiconductors for molecular probing,[1−3] spin-catalysis,[4] light-emitting diodes,[5−7] photovoltaic devices,[8,9] and information technologies.[10−12] Photoexcitation of organic semiconductors typically generates singlet (spin 0) states, which can be converted to triplet (spin 1) states via intersystem crossing (ISC). However, due to the spin selection rules, triplet formation is typically slow, and the deactivation often does not involve emission of a photon.[13] Triplets possess attractive properties such as low-lying energy levels,[14] long lifetime,[15] and extended diffusion length,[13] all of which are crucial in long-range energy and/or charge transfer schemes.[13,16−19]

Strategies to promote generation of triplet excitons predominately rely either on incorporation of heavy atoms into chromophores[20,21] or singlet fission.[22] Design of heavy-atom free organic compounds that result in enhanced ISC (EISC) is of great interest but remains a significant challenge. While singlet fission does not require heavy atoms, it is only

Received: August 8, 2018
Revised: October 15, 2018
Published: October 16, 2018

DOI: 10.1021/acs.chemmater.8b03366
Chem. Mater. 2018, 30, 7840−7851

observed in a handful of rigid and flat chromophores such as pentacene,[23] where energy of the triplet excited state (T_1) needs to be equivalent to half the energy of singlet excited state (S_1).[22,24−26]

In principle, incorporation of persistent radicals could also overcome the spin-forbidden nature of intersystem crossing[13] and provide an alternative opportunity for triplet sensitization.[16,27,28] Previous studies have shown that interactions between persistent radicals such as nitroxide and a chromophore result in fluorescence quenching of the chromophore.[29,30] The fluorescence quenching was attributed to the interactions of the excited singlet state of the organic chromophore with the persistent radicals.[31] In some cases, these interactions can result in coupling of electron spin of the radical that may lead to a series of spin states with various spin multiplicities.[32−36] Indeed, photoresponsive small molecules bearing stable radicals have illustrated inter-[37,38] or intramolecular[29,31] spin-based properties.[37,38] However, most of the early work focused on noncovalent radical and photoexcited chromophores[39−41] or ferromagnetism in conjugated polymers from intramolecular spin-exchange.[42−46] Thus, incorporation of persistent radicals to organic chromophores is expected to be a facile approach to control spin polarization in organic semiconductors, modulating excited states and ISC to harvest triplet energy for various technological applications.[16,17]

Generally, in the absence of a radical, emissive decay from singlet excited state of molecule A ($^1A^*$) to the ground state ^1A is the major pathway. The spin-forbidden ISC to the triplet excited state ($^3A^*$) is typically inefficient.[47] However, addition of a pendant radical R introduces various alternative possible decay pathways (Figure 1). A rapid depletion of $^1A^*$ and its

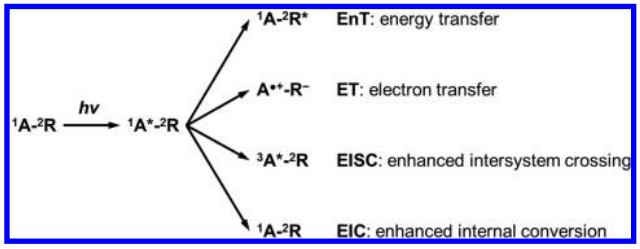

Figure 1. Common photophysical mechanisms for radical-induced decay pathways.

fluorescence quenching are commonly attributed to at least one of the following four photophysical mechanisms: (1) energy transfer (EnT) via Förster or Dexter process, (2) electron transfer (ET), (3) electron exchange-induced enhanced intersystem crossing (EISC), and (4) enhanced internal conversion (EIC). EnT from $^1A^*$ to R that forms an excited radical (R*) is typically presumed insignificant due to the low oscillator strength of their lowest energy n−π^* transition.[31] ET between $^1A^*$ and R can occur given appropriately matched redox potentials and can be experimentally verified by solvent dependence.[48,49] While studies have reported ET between nitroxide radicals and fullerene triplet states by noncovalent interactions,[50,51] interestingly only recently a study has demonstrated ET between phenoxyl radical to electron-deficient perylene diimide (PDI) due to the intramolecular charge transfer.[52] ET is commonly investigated in radical−donor−acceptor triad ensembles.[53−57] More recently, an internal ET between nitroxide radical side chains and electrochemically oxidized polythiophene backbone was reported.[58]

Incorporation of radicals may also lead to EIC, a mechanism that is less observed and studied. EIC is a competing process to EISC that leads to the recovery of the ground state ^1A. Therefore, if the goal is to harvest triplets, then the nonradiative EIC is an undesired process because the excitation energy dissipates in the form of heat. However, EIC can be useful in fluorescence sensing schemes or protecting unstable chromophores from photobleaching. For example, incorporation of a persistent radical to pentacene resulted in a dramatic improvement in the photostability as a result of deactivating the S_1 state of pentacene.[59] Surprisingly, only two examples have reported the quenching of the singlet state primarily due to EIC. The first example is fluorescamine dye with appended nitroxide radicals,[60] where the absence of triplet−triplet absorption and the unlikely energy transfer lead to the conclusion of EIC. The second example is the case of rubrene in the presence of TEMPO,[61] where the quenching of excited singlet state was attributed to EIC. The case of rubrene is contrary to most acenes where the presence of radicals is reported to result in large triplet yields.[59,62]

Paramagnetic radicals can enhance spin−orbit coupling and ISC, thus accelerating the formerly spin-forbidden process.[4] Most of the early work focused on interaction of freely diffusing radicals and chromophores in solutions.[39,63,64] Recently, radical-induced EISC has been demonstrated in few rigid chromophores including acenes,[35,62] fullerenes,[33,65] PDIs,[66,67] porphyrins,[36,68,69] BODIPYs,[27,70] and conjugated polymers.[44,71] Although these studies suggest radical−chromophore distance may influence the effectiveness of EISC, many essential structural factors such as conjugation length, type/number of radicals, electronic coupling, and geometrical influence have not been considered and are not entirely examined or understood. For example, the presence of a radical led to an entirely different quenching pathway in two separate studies of pentacene-nitroxides, where radical-induced EISC and singlet fission dominated in one case,[62] and in a separate case, the radical selectively interacted with triplet.[72] In the case of PDI-nitroxide radical, efficient EISC was observed in nonpolar solvent such as toluene, but ET was the major pathway in polar solvent such as THF.[66] These studies suggest that multiple photophysical mechanisms may compete in the same molecule and can greatly be influenced by many factors, thus highlighting the need for greater fundamental understanding of factors that influence and promote EIC or EISC. Furthermore, there are no obvious design rules based on structural or electronic parameters that are required to promote either an EIC or EISC mechanism or how to engineer excited state energy levels upon photoexcitation by incorporation of radicals.

Oligothiophenes and polythiophenes are among the well-studied class of organic semiconductors due to their strong absorption of visible light, ease of band structure engineering,[73] and strong self-assembly into nanostructure domains.[74,75] Polyalkylthiophenes are relatively stable and highly compatible with high-throughput production techniques, making them highly relevant for technological applications in field-effect transistors, sensors, and photovoltaics. Systematic studies of oligothiophenes have revealed that conjugation length of five or more repeating thiophene units can resemble the photophysical properties of polythiophenes.[76−78] Thus, we choose to study oligothiophenes with appended diradicals, to serve as a

DOI: 10.1021/acs.chemmater.8b03366
Chem. Mater. 2018, 30, 7840−7851

model system in probing excited-state dynamics, and to elucidate factors that promote either EIC or EISC.

In this Article, we report the synthesis, steady-state and ultrafast photophysics, magnetic properties, and single crystal X-ray diffraction of a series of oligothiophenes (**OTx**) and oligothiophenes with appended nitronyl nitroxide (NN) radicals (**RAx** and **RBx**) (Figure 2a). We employ computational modeling to establish a correlation of structural and electronic parameters that impact spin coupling and spin delocalization and determine general trends in predicting energy levels of excited-state and to further corroborate optical and ultrafast spectroscopy results. The design of **RAx** involves a progressive increase in the number of thiophene rings ranging from 2 to 6 covalently sandwiched between two NN radicals at α-terminal positions of the OT. In the **RBx** series, an additional *p*-phenylene linker was placed between the OT core and NN rings. This design allows us to elucidate structural factors such as conjugation length, electronic coupling, and geometrical influence on spin polarization and photoexcited spin state in organic semiconductors and gain fundamental understanding of photophysical processes that are unique to covalently joint radical−semiconductors chromophores. Our hypotheses are (i) incorporation of persistent radicals into π-conjugated organic semiconductors would result in spin coupling through π-conjugation and thus facilitate either EISC or EIC (Figure 2b); and (ii) the effectiveness of EISC or EIC will depend on the orbital overlap between the excited chromophore and singly occupied molecular orbital (SOMO) of the two NN radicals.

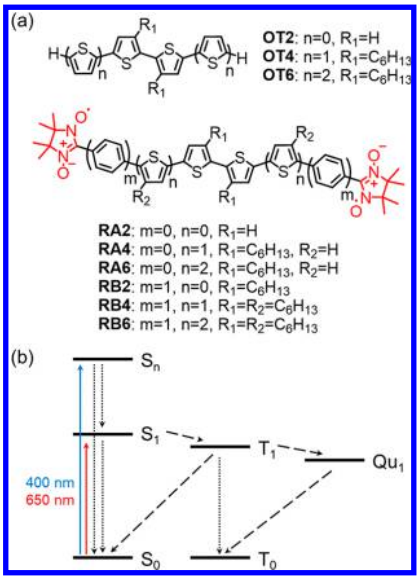

Figure 2. (a) Structures of oligothiophenes and diradicals. (b) Schematic energy diagram of diradicals, illustrating the photoexcitation and major decay processes of EIC (dotted arrows) and EISC (dashed arrows).

■ SYNTHESIS OF OT−NN DIRADICALS

Scheme 1 outlines the synthetic strategy to **RAx** and **RBx** series. Briefly, dialdehyde **A2** was prepared by deprotonation of bithiophene using *n*-BuLi followed by quenching with DMF. Compound **A2** was converted to **RA2** diradical in 27% yield in two steps: condensation with hydroxylamine **1** to form an aminoacetal intermediate, followed by oxidation with sodium periodate.[79] The poor solubility of longer OT without alkyl chains hindered further synthetic modifications and spectroscopic measurements; thus, we introduced *n*-hexyl chains to the backbone of oligothiophene diradicals. Hexyl side chains were installed in the head-to-head position of bithiophene rings using bis(trimethyltin) bithiophene **2**. This monomer served as a common precursor and a central building block for all other diradicals. Stille cross-coupling of **2** and a specific bromoaryl aldehyde **3a−e** afforded dialdehyde precursors **A4**, **A6**, **B2**, **B4**, and **B6** in 36−51% yields as orange to red crystals. The dialdehydes were first converted to aminoacetal intermediates by condensation with **1**. The aminoacetal intermediates were obtained as pale-yellow solids soluble in polar organic solvents. ^{1}H NMR of the crude condensation aminoacetal products in d_6-DMSO indicated the conversion from aldehyde (10 ppm) to aminoacetal (4.5 ppm). Oxidation of the aminoacetal intermediates with sodium periodate completed the synthetic sequence of diradicals and afforded **RA4**, **RA6**, **RB2**, **RB4**, and **RB6** in overall two-step yields of 24−46%. The diradicals were purified by column chromatography and obtained as dark green solids or crystals and characterized by mass spectrometry. All of the oligothiophene diradicals are generally stable when stored below 0 °C in the dark for at least a few months in solutions or as solids.

Scheme 1. Synthesis of Oligothiophene−Diradical RAx and RBx Series

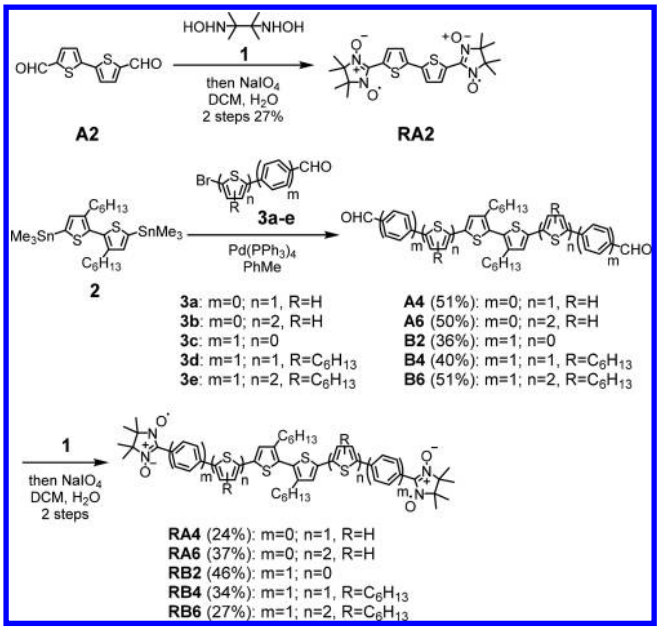

■ MAGNETIC PROPERTIES

Continuous-wave electron paramagnetic resonance (EPR) experiments at X-band (9.45 GHz) have been conducted on all diradicals and a phenyl nitronyl nitroxide (PhNN) monoradical (Figure S1). The EPR spectrum of PhNN represents an isolated radical, with a line shape that indicates two equivalent hyperfine couplings of the electron (S = 1/2) with the two ^{14}N nuclei (I = 1). The increase in the number of features and broadening in the **RA2** spectrum, with respect to PhNN, indicates an intramolecular electron−electron (e−e) interaction, which is consistent with the proposed structure and diradical nature of **RA2**. A relatively strong dipolar e−e interaction in **RA2** is indicated by the presence of a forbidden,

DOI: 10.1021/acs.chemmater.8b03366
Chem. Mater. 2018, 30, 7840−7851

$\Delta m_s = 2$, "half-field transition" (HFT), centered at 168.0 mT (Figure S1c,d). The intensity of the HFT is proportional to $1/r^6$, where r is the interspin distance.[80,81] The observation of the HFT for **RA2**, but not for **RA4** and **RA6**, is consistent with the small r value (~9.8 Å between N−N bridgehead positions, from the crystal structure), relative to **RA4** ($r \approx 19$ Å) and **RA6** ($r \approx 24.8$ Å). The broad, derivative line shape observed for **RA4**, **RA6**, **RB2**, and **RB4** is attributed to aggregation of these molecules in the frozen solid state in the $CHCl_3$/toluene solvent system used for the EPR measurements, possibly promoted by interactions of the hexyl chains. In contrast, **RB6** presents an EPR spectrum comparable to **PhNN**, as expected for the relatively large separation of the nitronyl nitroxide radical centers, $r \approx 33.4$ Å. The extended length and possible staggered, or off-axis, interactions among the six hexyl moieties in **RB6** may lead to separation of the radical centers.

To further study the intramolecular radical interactions, magnetic susceptibility (χ) of crystalline **RA6** was also obtained on a superconducting quantum interference device (SQUID) magnetometer, in the temperature range of 6−300 K at a constant magnetic field of 500 Oe. The magnetic susceptibility of **RA6** increased as the temperature decreased (Figure S2a), with no significant difference between zero-field cooled and field cooled profiles. According to the Curie−Weiss law, exchange interaction (θ) can be calculated based on the linear $\chi^{-1}-T$ plot (Figure S2b). Compared to the strong antiferromagnetic interactions in the thiophene−NN diradical ($\theta = -115$ K) and bithiophene−NN diradical ($\theta = -7.5$ K) analogs,[82] the two NN radicals in **RA6** exhibited a much smaller antiferromagnetic interaction ($\theta = -0.58$ K) due to the longer interspin distance.

CRYSTAL STRUCTURES

Understanding the molecular packing, topology, and orientation of the diradicals with respect to each other and with respect to the π-conjugated system would provide a fundamental understanding on the structural orientation and on the role of noncovalent interactions on spin-exchange and spin-alignment in organic semiconductors. Thus, we have obtained and investigated single-crystal X-ray structures of three oligothiophene-diradical oligomers **RA2**, **RA6**, and **RB4**.

Single crystal X-ray diffraction of **RA2** revealed a relatively planar backbone of oligothiophene with a torsion angle of 0.46° (Figure S3). The thiophene rings are relatively coplanar with the NN radical rings with a torsion angle of 1.95°. The small torsion angle provides efficient conjugation along the backbone thus facilitating reasonable spin-polarization transfer from the NN radical units to the bithiophene chromophore as observed from EPR results.

RA6 forms an asymmetric triclinic unit cell that contains two molecules with considerably different geometry (Figure 3a). In contrast to **RA2**, incorporations of long hexyl chains in the head-to-head position in the middle of **RA6** backbone results in a significant twist in the backbone resulting in a torsion angle of 64.57°. Each two adjacent thiophene rings are in an *s*-trans conformation with respect to the C−C single bond. Although the core thiophene units are highly twisted, the terminal thiophene units are relatively coplanar with NN rings with a torsion angle of 4°. The other conformation has a smaller central torsion angle of 38.54° (Figure S4), but the two pairs of thiophene rings involving C9−C10 and C17−C18 adopt the *s*-cis conformation around the C−C single bond to accommodate the bulky hexyl groups. Two **RA6** molecules in

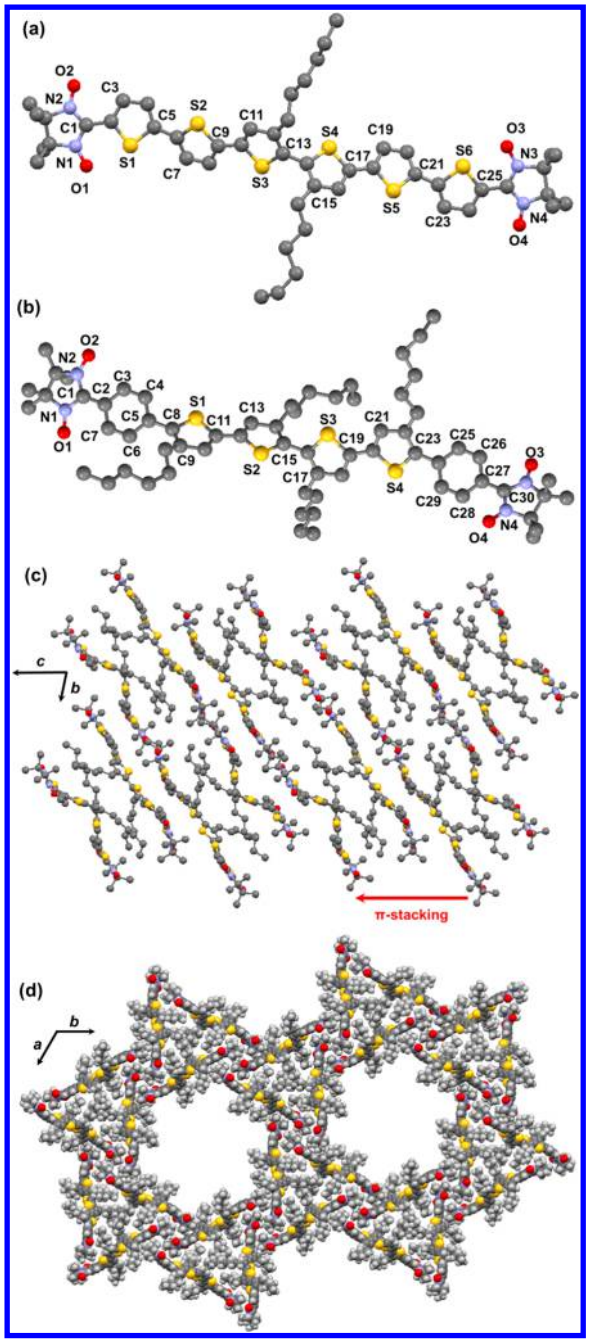

Figure 3. Molecular structures of (a) RA6 and (b) RB4 drawn as ball and stick models. (c) Crystal packing of **RA6** viewed down the *a*-axis, illustrating π-stacking along the 001 direction. (d) Crystal packing of **RB4** viewed down the *c*-axis, illustrating face-to-edge stacking that led to hexagonal voids.

an asymmetric unit embrace each other perpendicularly with a C13a−C14a−C13b−C14b dihedral angle of 92.97°. Both show an overall "saddle" shape with the saddle point at the middle of C13−C14. The thiophene rings of **RA6** form a face-to-face π-stacking with the adjacent asymmetric unit along the *c*-axis with an intermolecular distance of 3.43 Å (Figure 3c). The π-stacking also results in strong intermolecular coupling between the two NN−NN nitroxide radicals leading to 3.33 Å O···O distance between radicals across adjacent crystallographic unit cells. These interactions combined with the planar conformation between the NN radicals play a significant role in

DOI: 10.1021/acs.chemmater.8b03366
Chem. Mater. 2018, 30, 7840−7851

facilitating spin-coupling between the NN radicals and the terminal thiophene as predicted by computational modeling discussed later in the Computational Modeling Section.

RB4 crystal presents an intriguing yet complicated crystal packing system that is very reminiscent of organic cages. The crystal packing is different from the previous oligomers and is classified as a rhombohedral (*R*-3) trigonal crystal system. An asymmetric unit of triclinic **RB4** crystal contains one molecule (Figure 3b). **RB4** exhibit both a face-to-edge stacking (Figure 3d) and a slipped face-to-face stacking (Figure S6). The edge of the NN radical unit in **RB4** points to the phenylene ring, forming a face-to-edge configuration. Six **RB4** molecules in a unit cell organize in this fashion to form a closed shape three-dimensional hexagon, analogous to the cyclohexane chair conformation. This leads to a massive void with a 32.527 Å diameter surrounded by the hexyl chains. Oligothiophene core rings form a slipped face-to-face π-stacking along the *c*-axis with a relatively large intermolecular distance of 3.834 Å, suggesting an inefficient $\pi-\pi$ overlap. Similar to **RA6**, the largest torsion angle of 74.68° was found at the center of **RB4** presumably due to the head-to-head incorporation of the hexyl side chains. Interestingly, incorporation of the hexyl side chains in a tail-to-tail position into the two terminal thiophene units produces limited to no torsion in the molecular packing (torsion angle of −1.36°), resulting in relatively coplanar units. In **RB4**, the phenyl NN radicals are out of plane relative to the core oligothiophene units due to the torsion introduced by the *p*-phenylene linker (torsion angle of 42°), thus preventing any interactions between two adjacent NN diradicals on neighboring oligothiophenes or between the NN radicals and neighboring oligothiophene π-system, which is in stark contrast to **RA2** and **RA6**. Furthermore, the *p*-phenylene linker separates the oligothiophene core from the NN radical component by an average of 4.3 Å. The edge of the radical unit in one **RB4** molecule points to the face of the phenylene rings in another molecule to form a face-to-edge orientation.

STEADY-STATE OPTICAL SPECTRA

The steady-state absorption and emission data of **OTx**, **RAx**, and **RBx** series in dilute toluene solution are shown in Figure 4

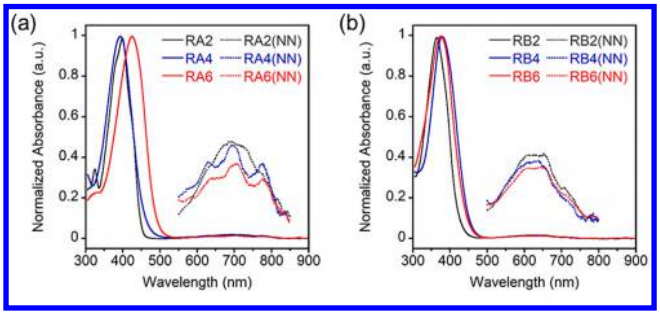

Figure 4. Steady-state optical absorption spectra of (a) **RAx** and (b) **RBx** series in PhMe, and enlarged NN radical absorption features near 700 nm (insets).

and summarized in Table 1. **OTx** series show one main absorption peak with absorption maximum (λ_{max}) at 305−390 nm assigned to the $\pi-\pi^*$ transition. As expected, an increase in the conjugated length in the **OTx** series results in a clear red-shift in the absorption. In contrast, both **RAx** and **RBx** show two main absorption peaks (Figure 4): the peak with λ_{max} at 365−425 nm is attributed primarily to the $\pi-\pi^*$ transition,

Table 1. Spectral Profiles of OT Nonradicals and Diradicals in PhMe[a]

cpd	λ_{max} (nm)	ε_{OT} ($M^{-1}cm^{-1}$)	λ_{NN} (nm)	λ_{max}^{em} (nm)	ϕ_F
OT2	305	1.17×10^4		367	0.016
OT4	344	3.36×10^4		478	0.16
OT6	390	5.11×10^4		512	0.43
RA2	402	3.83×10^4	686		
RA4	393	3.69×10^4	693		
RA6	425	5.35×10^4	707		
RB2	365	5.15×10^4	653		
RB4	379	3.25×10^4	639		
RB6	376	1.38×10^5	650		

[a]Notes: λ_{OT} and ε_{OT} are the wavelength and extinction coefficient of the peak associated with the OT core, respectively. λ_{NN} is the peak wavelength associated with the NN radical. ϕ_F is the fluorescence quantum yield calibrated with rhodamine 6G (ϕ_F = 0.95 in EtOH). Fluorescence of the diradicals are too weak to be recognized.

and weak absorption peaks are observed at 639−707 nm with vibronic structures. The low-energy absorption peaks are unique to OT−NN radicals, which may suggest they correspond to n−π^* transition and have previously been assigned to that transition.[62,83] However, an increase in the solvent dielectric (PhMe, THF, and MeCN) did not result in a hypsochromic shift as typically observed with n−π^* transitions. In general, incorporation of the diradicals to oligothiophene **RAx** series leads to a bathochromic shift in λ_{max} by 30−100 nm. This red-shift is attributed to a direct conjugation with the double NN radical units. This is further supported by the crystal structures of **RA2** and **RA6**, which show that the NN radical rings are essentially coplanar with adjacent thiophene rings, thus contributing to significant orbital overlap. However, the λ_{max} in all three **RBx** radicals appeared blue-shifted compared to the **RAx** counterparts with the same number of thiophenes. This blue shift can be explained by the crystal structure of **RB4**, which shows a large torsion angle of 74.68° at the center of **RB4** thereby reducing the effective conjugation length.

All of the **OTx** series show optical photoluminescence (PL) with a significant red-shift in the emission maximum and an increase in fluorescence quantum yield (ϕ_F) as a result of an increase in the number of thiophene rings (Table 1), corresponding to a similar trend reported for similar oligothiophenes.[77,78] The low ϕ_F of **OT2** is attributed to an efficient ISC from S_1 to T_4.[84,85] However, incorporation of diradicals into OT results in complete quenching of fluorescence in **RAx** and **RBx** (Figure S7). Detailed mechanisms are studied by computational modeling and TA spectroscopy and discussed in the following sections.

COMPUTATIONAL MODELING

Density functional theory (DFT) and second-order multi-reference perturbation theory based on the driven similarity renormalization group (DSRG-MRPT2)[86,87] were employed to study structural and electronic factors that influence spin-coupling and predict excited-state energy levels. In the OT−NN diradicals, coupling of the unpaired spins on the two NN radicals (^{2}NN) will yield a near-degenerate singlet or triplet ground state, depending on the sign of the spin-exchange coupling. The low-lying excited states of OT−NN formally arise from the mixing of singlet and triplet excited OT (^{1}OT*/^{3}OT*) and two ^{2}NN radicals to generate a variety of

DOI: 10.1021/acs.chemmater.8b03366
Chem. Mater. 2018, 30, 7840−7851

states of singlet (S, spin 0), triplet (T, spin 1), and quintet (Qu, spin 2) multiplicities.[35,36] Because DFT cannot correctly describe the multideterminant nature of these states, computations of the relative energies of **RAx** and **RBx** species were performed with the DSRG-MRPT2 approach (see Supporting Information for details).

Geometries and spin densities for selected **RAx** and **RBx** species were obtained with DFT using B3LYP functional[88,89] and the def2-SVP basis set.[90] To simplify the computational modeling of these species, we omitted the hexyl side chains. Due to the small singlet−triplet gap of these species, all DFT computations targeted the lowest triplet spin state. The HOMO and LUMO from DFT of all four oligothiophene-diradicals (**RA2**, **RA4**, **RB2**, and **RB4**) are delocalized on the oligothiophene cores, whereas the two SOMOs are localized mainly on the nitroxide five-membered NN ring (Figures 5 and

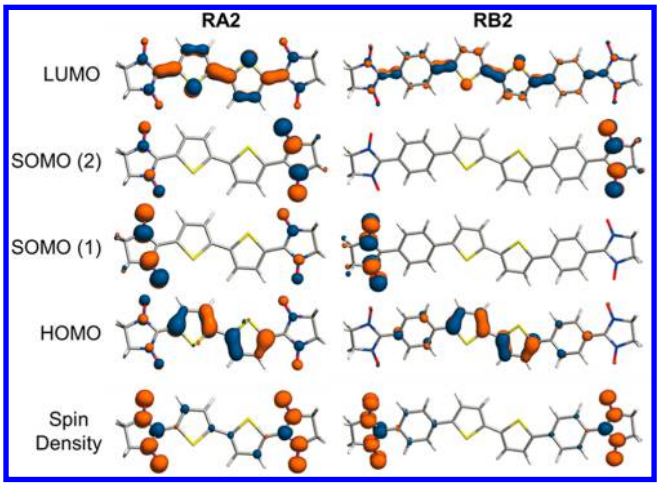

Figure 5. Molecular orbitals and spin density of triplet **RA2** and **RB2**, obtained from B3LYP/def2-SVP level computations (hexyl groups omitted).

S8). Interestingly, the calculated spin density distributions of **RA2** and **RA4** reveal some delocalization of the spin density along the thiophene units adjacent to the NN five-membered rings, although the largest spin coefficients are found on the NN−radical substituents (Figures 5 and S8). In contrast, the spin density on **RB2** and **RB4** does not extend to the thiophene units but rather is localized on the NN unit with minor contribution on the adjacent *p*-phenylene unit. This suggests that the delocalization of spin density is confined to a very short distance of 4.3 Å despite the conjugated nature of the *p*-phenylene ring. These results are also consistent with experimental results obtained from crystal structure X-ray diffraction, which indicates a torsion angle of 42° between the *p*-phenylene ring and the radical units that would quench electron delocalization.

It is noteworthy that DSRG-MRPT2 predicts for **RA2**, **RA4**, and **RA6** very small singlet−triplet energy gaps ($\Delta E_{ST} = E_T - E_S$) of +0.57, +0.06, and −0.03 kcal/mol, respectively. The larger ΔE_{ST} of **RA2** is corroborated by strong spin interactions observed in the EPR and the relatively high antiferromagnetic coupling measured with SQUID, suggesting that the thiophene rings facilitate strong spin coupling between the two NN rings. In the case of **RA4** and **RA6**, the small ΔE_{ST} implies that at 298 K the population of the S_0 and T_0 states is near statistical. The small singlet−triplet gap of these diradicals is in accordance with topological effects on radical interactions where coupling strength decreases rapidly with long interspin distance.[71,91] The radicals in **RA6** are 24 Å apart and therefore in a weak coupling regime,[92,93] a result consistent with the small degree of exchange interactions between the two unpaired electrons observed in EPR experiments.

Predicted excited-state energy levels of **OTx** (**OT2**, **OT4**, and **OT6**) and **RAx** (**RA2**, **RA4**, and **RA6**) computed with the DSRG-MRPT2 are shown in Figures 6 and S9. In accordance

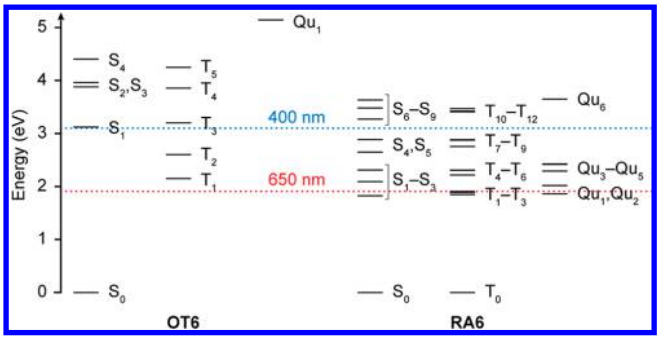

Figure 6. Energy diagram of **OT6** and **RA6** computed at the DSRG-MRPT2/def2-SVP level. Energies corresponding to 400 nm (blue) and 650 nm (red) photoexcitation are indicated with dotted lines.

with experimental results, an increase in conjugation length of **OTx** leads to a decrease in energy levels of the first singlet and triplet excited states. We also note that the S_1 and T_1 energy levels calculated for **OT6** (Figure 6) correspond well to the value measured in absorption and PL (Table 1) spectra and reported in the literature.[84] As expected for a closed-shell structure, the quintet excited state Qu_1 of **OT6** is substantially higher in energy than S_1 or T_1 (>5 eV).

In stark contrast, incorporation of diradicals results in complicated energy diagrams for **RAx** series with a number of additional singlet, triplet, and quintet states that are close in energy (Figures 6 and S9). For example, while **OT2** shows only three excited states below 5 eV, incorporation of the NN radicals (**RA2**) results in more than 20 low-lying near-degenerate singlet and triplet states (Figure S9). This suggests that both ISC and IC are viable decay mechanisms and that, perhaps, competition between the two leads to diminishing EISC in **RA2**. The calculated vertical excitation energies of **RA2** are also consistent with the experimental absorption energies. The most intense transitions are found at higher energies (f_{osc} = 1.169 at 336 nm) and correspond to an OT $\pi-\pi^*$ excitation, whereas the lowest-energy transitions are weaker (f_{osc} = 0.039 at 401 nm, f_{osc} = 0.005 at 503 nm) and show contributions from multiple excitations (e.g., π-SOMO, SOMO-π^*).

In the case of **RA6**, DSRG-MRPT2 computations assigned the experimental absorption maximum (λ_{max} = 425 nm) to an OT $\pi-\pi^*$ excitation (Table S6). Since S_0 and T_0 are both populated at room temperature, this band is predicted to be a statistical mixture of the S_0-S_5 (singlet manifold) and the T_0-T_9 (triplet manifold) transitions. Various lower excited states can provide many decay pathways from S_5 and T_9. The S_4 state has a ^{3}OT* character and opposite spins on the NN radicals, while the low-lying singlet excited states S_1-S_3 involve charge transfer (CT) between OT and NN. Similar electronic configurations were found for triplet states T_2-T_3, and the first triplet excited state T_1 corresponds to the ^{3}OT* with two

DOI: 10.1021/acs.chemmater.8b03366
Chem. Mater. 2018, 30, 7840−7851

radicals of opposite spin. The first quintet state Qu_1 has almost identical energy to S_1/T_1 and consists of ^{3}OT* with spin aligned with that of the two radicals. To understand the importance of the side chains in **RA6**, we studied a model in which the hexyl groups are replaced with methyl groups. Introduction of the methyl groups leads to a large twist in the molecular backbone (torsion angle of 51.1°), which is in good agreement with the one observed in the crystal structure. However, the electronic properties are nearly unchanged: excitation energies of the **RA6** model shift at most by 0.2 eV when the methyl groups are introduced. For other OT−NN radicals, computations also revealed the degenerate singlet/triplet ground states and additional excited states (Figure S9). For example, the lowest excited states of **RA4** consist of the near-degenerate S_1, T_1, and Qu_1, all found around 2 eV above the ground state. Although with different spin multiplicities, these excited states may not be well distinguished from each other in optical spectra.[66]

Overall, our computational results suggest that the NN radicals provide many possible routes for both EIC and EISC, thus quenching the original OT fluorescence. The additional low-lying singlet states allow extra decay pathways after direct excitation of ^{1}OT*. Meanwhile, excited states in triplet or quintet manifold with similar energy could facilitate the ISC from the singlet states.

TRANSIENT ABSORPTION

To further understand the fluorescence quenching in oligothiophene diradicals and to probe the excited-state dynamics and kinetics of **RAx** and **RBx**, we used femtosecond and nanosecond transient-absorption (TA) spectroscopy, correlated with steady-state photophysics, molecular packing from the single-crystal X-ray diffraction, and the computational study. We initially investigated the photoexcitation of the **OTx** as a reference to compare to oligothiophene−diradicals series (**RAx** and **RBx**). Figure S10 shows the photoexcitation of **OT** series, exemplified by **OT6**, with 400 nm laser pulse generating the ground state bleaching (overlapped with pump wavelength) and stimulated emission at 450−600 nm as negative features. Decay of S_1 would follow the common pathways for closed-shell molecules: return to ground state S_0 via fluorescence and internal conversion, or cross to T_1 via ISC. The transient spectra of the **OTx** series was fit into two exponential decay components (Table 2): a faster decay component associated with a broad absorption band with a maximum near 850 nm (τ = 361 ps), and a slower component that emerged at 695 nm and continued to rise throughout 1 ns after photoexcitation. In nanosecond TA spectra of **OT6**, this 690 nm peak persisted through a decay time constant of τ = 1.54 μs and was the only main feature observed at the μs-time scale. The 850 nm peak corresponds to the singlet excited state (^{1}***OT**) absorption of **OT6**, while the 695 nm peak was identified as the triplet excited state (^{3}*OT) absorption.[77] Transient spectra of **OT2** and **OT4** were obtained in a similar manner and show essentially the same trend. In general, the ^{1}*OT decay time constant (τ) increased by 10-fold as the number of oligothiophene units increased in the OTx series, while the ^{3}*OT decay time constant decreased by up to 10-fold (Table 2). These results are consistent with literature values of nonalkyl OTx, which have no apparent solvent dependence.[70] That is, an increase in OTx length results in a decrease in the rate constant of ISC (k_{ISC}),[77] thus leading to longer ^{1}*OTx lifetime and high fluorescence quantum yield (ϕ_F) in **OT6** compared to that of **OT2**. For example, **OT2** exhibits the longest ^{3}*OT lifetime in the OTx series due to the large T_1-S_0 energy gap and reduced Franck−Condon overlap.[77]

The femtosecond and nanosecond TA spectra and kinetics of **RAx** and **RBx** are shown in Figures 7 and S11. Decay

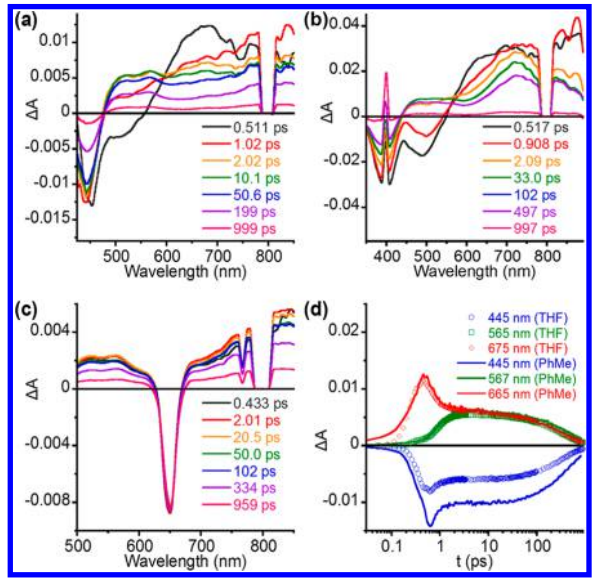

Figure 7. Femtosecond transient absorption spectra at indicated times of (a) **RA6** and (b) **RB4** in PhMe following a 400 nm laser pulse. (c) **RA6** in PhMe following a 650 nm laser pulse. (d) Comparison of decay kinetic profiles of **RA6** obtained in THF and PhMe.

Table 2. Transient Absorption Kinetics in PhMe at 293 K

cpd	τ_1 (ps)	τ_2 (ps)	τ_3 (ns)	λ for τ_3 (nm)
OT2	46[77]		1.46×10^5[77]	380
OT4	490[77]		4.80×10^4[77]	560
OT6	361 ± 4		1540 ± 10	690
RA2	0.243 ± 0.013	272 ± 6	105 ± 40	420
RA4	0.543 ± 0.053	468 ± 5	353 ± 613	680
RA6	0.474 ± 0.019	324 ± 8	192 ± 8	760
RB2	0.651 ± 0.08	399 ± 3	n/a	n/a
RB4	1.09 ± 0.04	346 ± 7	29.7 ± 136.5	690
RB6	3.12 ± 0.14	450 ± 11	27.0 ± 4.1	730

constants of **RAx** and **RBx** series are summarized in Table 2. Photoexcitation of **RAx** and **RBx** with 400 nm excitation laser generated a sharp negative peak in the range of 400−450 nm, corresponding to the ground state bleach and weak stimulated emission at 450−550 nm as negative features (Figures 7 and S11). In general, the stimulated emission of **RAx** and **RBx** was significantly weaker than that in **OTx** and only existed through the very early stage (<1 ps) as an implication of the rapid initial decay. This is consistent with the effective quenching observed by steady-state PL. The negative stimulated emission feature was noticeably more prominent in the **RBx** series than **RAx**, indicative of strong OT−NN electronic coupling in **RAx** as predicted by the computation study and elucidated by the single crystal X-ray diffraction.

Based on the experimental and predicted excited-state energy levels, photoexcitation with the 400 nm laser would populate high singlet-excited state (S_n) instead of S_1 (the

DOI: 10.1021/acs.chemmater.8b03366
Chem. Mater. 2018, 30, 7840−7851

lowest excited-state energy level) in both **RAx** and **RBx**. For example, in the case of **RA6**, the directly populated state would be S_5 as predicted by DFT calculations (Figure 5). In the femtosecond TA spectra of **RAx** and **RBx** exemplified by **RA6** (Figure 7a), the negative feature of emission centered at 510 nm disappeared within 1 ps, an implication of rapid depletion of S_5. Meanwhile, the initial absorption at 665 nm seen in Figure 7a emerged within the instrument response time (~100 fs) and gave way to a broad positive feature across almost the entire spectral window up to 1200 nm (Figure S12a). This could be the transition feature of S_1 to S_n. The TA spectra after 1 ps appeared differently from the early stage, suggesting depopulation of S_5 by EIC or EISC. A simultaneous rise was observed at 567 and 837 nm before the full recovery of ground state bleaching at 445 nm within 1 ns.

Figure 7d shows kinetics of **RA6** at 665 nm fits a double component exponential decay with time constants of τ_1 = 0.474 ps and τ_2 = 324 ps. Decay constants and kinetics of **RA6** are summarized in Table 2. Kinetics of the 567 nm peak fit a monoexponential decay of 473 ps and is largely synchronized with the slower decay process observed at 665 nm. Features observed at 950 nm (Figure S12a) were fitted with the biexponential decay time constants of 0.795 and 522 ps at 950 nm and generally in line with the same kinetics of the 665 nm. Decay time constants τ_1 and τ_2 calculated for **RA6** are faster by 900-fold and 8 × 10^3-fold, respectively, compared to the intrinsic singlet lifetime of **OT6** (361 ps). Time constant of τ_1 is more consistent with IC time scale and presumably corresponds to the decay of S_5 to S_1. We further attribute τ_2 to the nonradiative decay of S_1 to S_0. To further verify this assignment and study the nature of the λ_{NN} peaks at 700 nm observed in the steady-state optical absorption, we probed **RA6** with a 650 nm excitation laser (Figure 7c). Higher concentration (×10) and more powerful laser pulse (×10^3) were required to compensate for the low extinction coefficient (~10^2 M^{-1} cm^{-1}). Spectral profiles throughout the measurement consistent with the late (>2 ps) spectra observed using 400 nm excitation laser were also observed (Figure 7c). Lack of early stage emission with 1 ps suggests that photoexcitation at 650 nm is unable to access the S_5 state. This is further evidence that photoexcitation at 400 nm of **RA6** leads to S_5−S_1 transition, followed by a decay of S_5 to S_1 and then to S_0 by internal conversion. Thus, we assign the λ_{NN} absorption peak at 700 nm to the S_0−S_1 transition. It is noteworthy that the stimulated emission of the **RAx** and **RBx** series arises only from higher energy wavelength of 450−550 nm rather than the weak low energy λ_{NN} absorption at 639−707 nm, which appears to be an exception to Kasha's rule.[94] As the typical exception of this rule, azulene is similar to these oligothiophene−diradicals in the way of having a small S_0−S_1 gap and a large S_1−S_n gap (S_n as the state directly accessed by 400 nm excitation).[95] The energetically close S_1 and ground state facilitates rapid nonradiative decay of S_1, while the majority of the slower radiative process takes place from the higher excited state S_n.

Similarly, rapid initial decay (τ_1 = 0.2−3.2 ps) was observed in all **RAx** and **RBx** diradicals, compared to the intrinsic lifetime of ^{1}OT* (46−490 ps).[77] In contrast to **OTx**, an increase in the number of thiophenes in **RAx** did not influence the excited state spectral features or decay time constants. In contrast, an increase in the number of thiophenes in the **RBx** series (Figure 7b) resulted in a progressive decrease in τ_1 decay time constant and was slower than **RAx** by factors of 2−7. From a molecular structure perspective, this can be attributed to the additional *p*-phenylene spacers and hexyl groups. Each *p*-phenylene in **RBx** increases OT−NN distance by 4.3 Å, while both *p*-phenylene and hexyl groups can disrupt the conjugation, reducing the OT−NN electronic coupling and therefore the impact of radicals to the excited OT.

Nanosecond TA spectra of **RAx** and **RBx** radicals were also recorded to probe the possible EISC to T_1 or Qu_1 excited states. In all six molecules of oligothiophene−diradicals with the exception of **RA6**, only residual features of the S_1 decay with a subnanosecond time constant τ_2 were observed as a result of early photoexcitation at the 400 nm (Figures S12b and S13). In the case of **RA6**, while the S_1 decay with a subnanosecond time constant τ_2 was the dominant feature (Figure S12b), a long-lived (τ_3 = 192 ns) positive feature with a very low amplitude at 760 nm appeared at 3 ns. We assign this long-lived feature to ^{3}OT* in **RA6**. We note that the ^{3}OT* in **RA6** is significantly red-shifted compared to ^{3}OT* in **OT6**, presumably due to extended conjugation with NN radicals. Radicals are also known to accelerate the triplet decay,[62,72] so τ_3 is reasonable for the ^{3}OT* component in **RA6**, even though it is shorter than the **OT6** counterpart. In the biexponential fitting, the τ_3 component only made up less than 5% of the amplitude, and the remainder was from the τ_2 component. Moreover, the ground state has almost fully recovered by the time S_1 features vanished, further indicating the minority of the τ_3 component. In the nanosecond TA spectra of all other oligothiophene−diradicals, this τ_3 process was essentially indistinguishable from the background. These results suggested that EISC cannot be a major decay pathway in **RAx** and **RBx** series.

Other photophysical mechanisms discussed in the introduction are also evaluated based on results of OT−NN radicals. Among all common pathways, singlet fission is unlikely due to the low concentration for fluorescence measurements (<10^{-4} M) and long intermolecular distance.[23] The effectiveness of Förster resonance energy transfer (FRET) is primarily determined by the spectral overlap between the donor emission and acceptor absorption.[96] Only **OT6** has a moderately high ϕ_F (0.43) and spectral overlap, but the low extinction coefficient of λ_{NN} disfavors FRET. For the same reason, Dexter-type EnT is also unlikely despite the short OT−NN distance.[66]

Electron transfer typically exhibits strong solvent dependence;[66,67] therefore, tuning the solvent polarity could effectively probe whether ET is operative in the nonradiative decay of excited states. The CS free energy change (ΔG_{CS}) in PhMe and THF was calculated for **RA6** from the Rehm−Weller equation (eq S1).[97] CS free energy change for **RA6** is found to be thermodynamically more favorable in THF (ΔG_{CS} = −0.99 eV) than in nonpolar PhMe (ΔG_{CS} = −0.21 eV), and both are in Marcus normal region. Furthermore, decay kinetics profile in THF and PhMe are essentially identical (Figure 7d). In addition, if there was ET between the oligothiophene and the NN radical rings, one would expect that features in the TA spectra and time constants would shift as a function of increasing the number of thiophenes due to distinct OT radical cation features reported previously.[98] Thus, we rule out the possibility of ET as a major mechanism for fluorescence quenching.

Together, the steady-state optical absorption, computation study, and ultrafast transient absorption suggest EIC is responsible for the rapid decay in **RAx** and **RBx** diradical series with very minimal ISC ^{3}OT* formation in **RA6**. There

DOI: 10.1021/acs.chemmater.8b03366
Chem. Mater. 2018, 30, 7840−7851

are two major factors that contributed to EIC as a result of incorporation of the diradicals: (i) coupling of the NN radicals and oligothiophene results in new low-lying singlet and triplet states that act as "trap states" and contribute to making EIC the dominant decay pathway rather than ISC. (ii) The incorporation of the diradicals generates multiple S_n and T_n states that are near-degenerate in energy as predicted by the computation study (Figures 6 and S9). Even if there is ISC from S_n to T_m, T_m decays back very fast to T_1 and eventually to T_0 via IC. This is illustrated by the example of **OT2** and its analogue **RA2**. In the case of bithiophene **OT2**, ISC is essentially quantitative without incorporation of diradicals, and that is largely due to the small energy gap between S_1 and T_3.[84] However, **RA2**/**RB2** diradicals show very short-lived species, suggesting that either the low-lying S_1 provides a more favorable pathway with no change in spin multiplicity or a change in spin multiplicity to T_n decays to the ground state by IC.

In general, **RBx** shows slower EIC compared to **RAx**. This observation can be explained by the computational study and molecular packing from the single-crystal X-ray diffraction where additional phenylene ring spacer limits spin-polarization to the OT core. These results suggest that for efficient spin-polarization to occur one or more of the following requirements are needed: (1) significant orbital overlap between the π-system and the radical centers is required, (2) short distance between the radical and π-system need to be maintained (<4.3 Å), and (3) intermolecular interactions between the radical centers and the OT π-system must occur.

CONCLUSIONS

In summary, we synthesized a series of oligothiophenes and oligothiophenes with covalently linked nitronyl nitroxide diradicals. Incorporation of the diradicals results in unusual excited-state dynamics and interesting photophysical and magnetic properties. In all cases, incorporation of NN diradicals results in fluorescence quenching. A computational study predicted that the OT−NN series have very small singlet−triplet energy gaps, where the largest ΔE_{ST} is predicated in **RA2** and is corroborated by strong spin interactions observed in the EPR and the relatively high antiferromagnetic coupling measured with SQUID, suggesting that the thiophene rings facilitate strong spin coupling between the two NN rings. In contrast, an increase in the distance between the diradicals results in small ΔE_{ST}, which implies that at 298 K the population of the S_0 and T_0 states is near statistical, consistent with the small degree of exchange interactions between the two unpaired electrons observed in EPR and SQUID experiments. Incorporation of the NN diradicals results in more than 20 low-lying near-degenerate singlet (spin 0), triplet (spin 1), and quintet (spin 2). Optical spectral results concluded that the absorption with low extinction coefficient associated with NN was the transition to low-lying singlet and triplet states. Due to the electronic coupling in OT−NN diradicals, the OT associated absorption was no longer the transition from ground state to S_1, but to a higher singlet state, such as S_5 of **RA6**. The S_1 and several other low-lying states provide several pathways to deactivate S_5. The increased OT−NN distance in **RBx** by a phenyl unit reduced the electronic coupling and led to slower decay. Although the lowest quintet Qu_1 state lies slightly below S_1 and T_1, no definitive ^{3}OT* optical absorption feature was observed from nanosecond TA spectra of the diradicals.

ASSOCIATED CONTENT

Supporting Information

The Supporting Information is available free of charge on the ACS Publications website at DOI: 10.1021/acs.chemmater.8b03366.

Full details of synthetic procedures and additional synthetic schemes showing preparation of key precursors, intermediates, and final products, and characterization data including ^{1}H NMR, ^{13}C NMR, and high resolution mass; continuous-wave X-band EPR spectra; SQUID spectra of **RA6**; additional figures of X-ray single crystal structures of **RA2**, **RA6** and **RB4** and the corresponding crystallographic data tables; steady-state photoluminescence spectra; DFT modeling of molecular orbitals, spin density, and energy levels; Femto- and nanosecond transient absorption spectra (PDF)

Crystallographic information for **RA2** (CIF), **RA6** (CIF), and **RB4** (CIF)

AUTHOR INFORMATION

Corresponding Authors

*E-mail: francesco.evangelista@emory.edu.
*E-mail: tlian@emory.edu.
*E-mail: ee30@rice.edu.

ORCID

Chenyang Li: 0000-0002-0059-4174
Kurt Warncke: 0000-0002-3587-3720
Francesco A. Evangelista: 0000-0002-7917-6652
Tianquan Lian: 0000-0002-8351-3690
Eilaf Egap: 0000-0002-6106-5276

Notes

The authors declare no competing financial interest.

ACKNOWLEDGMENTS

This work was supported by NSF grant CHE-1821863 (to E.E.), CHE-1709182 (to T.L.), DOE grant DE-SC0016004 (to F.A.E), and by a Research Fellowship of the Alfred P. Sloan Foundation (to F.A.E.). The authors also appreciate Dr. John Bacsa for X-ray crystallography data collection and analysis, and Dr. Jianhua Li for help with the SQUID experiments.

REFERENCES

(1) Hughes, B. K.; Braunecker, W. A.; Ferguson, A. J.; Kemper, T. W.; Larsen, R. E.; Gennett, T. Quenching of the Perylene Fluorophore by Stable Nitroxide Radical-Containing Macromolecules. *J. Phys. Chem. B* **2014**, *118*, 12541−12548.

(2) Li, P.; Xie, T.; Duan, X.; Yu, F.; Wang, X.; Tang, B. A New Highly Selective and Sensitive Assay for Fluorescence Imaging of · OH in Living Cells: Effectively Avoiding the Interference of Peroxynitrite. *Chem. - Eur. J.* **2010**, *16*, 1834−1840.

(3) Yapici, N. B.; Jockusch, S.; Moscatelli, A.; Mandalapu, S. R.; Itagaki, Y.; Bates, D. K.; Wiseman, S.; Gibson, K. M.; Turro, N. J.; Bi, L. New Rhodamine Nitroxide Based Fluorescent Probes for Intracellular Hydroxyl Radical Identification in Living Cells. *Org. Lett.* **2012**, *14*, 50−53.

(4) Buchachenko, A. L.; Berdinsky, V. L. Electron Spin Catalysis. *Chem. Rev.* **2002**, *102*, 603−612.

(5) Nguyen, T. D.; Ehrenfreund, E.; Vardeny, Z. V. Spin-Polarized Light-Emitting Diode Based on an Organic Bipolar Spin Valve. *Science* **2012**, *337*, 204−209.

(6) Wang, J.; Chepelianskii, A.; Gao, F.; Greenham, N. C. Control of Exciton Spin Statistics through Spin Polarization in Organic Optoelectronic Devices. *Nat. Commun.* **2012**, *3*, 1191.

DOI: 10.1021/acs.chemmater.8b03366
Chem. Mater. 2018, 30, 7840−7851

(7) Peng, Q.; Obolda, A.; Zhang, M.; Li, F. Organic Light-Emitting Diodes Using a Neutral π Radical as Emitter: The Emission from a Doublet. *Angew. Chem., Int. Ed.* **2015**, *54*, 7091−7095.
(8) Zhang, Y.; Basel, T. P.; Gautam, B. R.; Yang, X.; Mascaro, D. J.; Liu, F.; Vardeny, Z. V. Spin-Enhanced Organic Bulk Heterojunction Photovoltaic Solar Cells. *Nat. Commun.* **2012**, *3*, 1043.
(9) Wang, F.; Vardeny, Z. V. Organic Spin Valves: The First Organic Spintronics Devices. *J. Mater. Chem.* **2009**, *19*, 1685−1690.
(10) Rajca, A.; Wongsriratanakul, J.; Rajca, S. Magnetic Ordering in an Organic Polymer. *Science* **2001**, *294*, 1503−1505.
(11) Yonekuta, Y.; Susuki, K.; Oyaizu, K.; Honda, K. Battery-Inspired, Nonvolatile, and Rewritable Memory Architecture: A Radical Polymer-Based Organic Device. *J. Am. Chem. Soc.* **2007**, *129*, 14128−14129.
(12) Troiani, F.; Affronte, M. Molecular Spins for Quantum Information Technologies. *Chem. Soc. Rev.* **2011**, *40*, 3119−3129.
(13) Bardeen, C. J. The Structure and Dynamics of Molecular Excitons. *Annu. Rev. Phys. Chem.* **2014**, *65*, 127−148.
(14) Yersin, H.; Rausch, A. F.; Czerwieniec, R.; Hofbeck, T.; Fischer, T. The Triplet State of Organo-Transition Metal Compounds. Triplet Harvesting and Singlet Harvesting for Efficient OLEDs. *Coord. Chem. Rev.* **2011**, *255*, 2622−2652.
(15) Romero, N. A.; Nicewicz, D. A. Organic Photoredox Catalysis. *Chem. Rev.* **2016**, *116*, 10075−10166.
(16) Schmidt, T. W.; Castellano, F. N. Photochemical Upconversion: The Primacy of Kinetics. *J. Phys. Chem. Lett.* **2014**, *5*, 4062−4072.
(17) Kamkaew, A.; Lim, S. H.; Lee, H. B.; Kiew, L. V.; Chung, L. Y.; Burgess, K. BODIPY Dyes in Photodynamic Therapy. *Chem. Soc. Rev.* **2013**, *42*, 77−88.
(18) Shockley, W.; Queisser, H. J. Detailed Balance Limit of Efficiency of *P-n* Junction Solar Cells. *J. Appl. Phys.* **1961**, *32*, 510−519.
(19) de Wild, J.; Meijerink, A.; Rath, J. K.; van Sark, W. G. J. H. M.; Schropp, R. E. I.; Nelles, G.; Yasuda, A.; Chernov, S.; Aleshchenkov, S.; Cheprakov, A.; et al. Upconverter Solar Cells: Materials and Applications. *Energy Environ. Sci.* **2011**, *4*, 4835−4848.
(20) Turro, N. J.; Kavarnos, G. J.; Cole, T.; Scribe, P.; Dalton, J. C. Molecular Photochemistry. XXXIX. External Heavy-Atom-Induced Spin-Obital Coupling. Spectroscopic Study of Naphthonorbornanes. *J. Am. Chem. Soc.* **1971**, *93*, 1032−1034.
(21) Koziar, J. C.; Cowan, D. O. Photochemical Heavy-Atom Effects. *Acc. Chem. Res.* **1978**, *11*, 334−341.
(22) Smith, M. B.; Michl, J. Singlet Fission. *Chem. Rev.* **2010**, *110*, 6891−6936.
(23) Walker, B. J.; Musser, A. J.; Beljonne, D.; Friend, R. H. Singlet Exciton Fission in Solution. *Nat. Chem.* **2013**, *5*, 1019−1024.
(24) Jundt, C.; Klein, G.; Sipp, B.; Le Moigne, J.; Joucla, M.; Villaeys, A. A. Exciton Dynamics in Pentacene Thin Films Studied by Pump-Probe Spectroscopy. *Chem. Phys. Lett.* **1995**, *241*, 84−88.
(25) Zirzlmeier, J.; Lehnherr, D.; Coto, P. B.; Chernick, E. T.; Casillas, R.; Basel, B. S.; Thoss, M.; Tykwinski, R. R.; Guldi, D. M. Singlet Fission in Pentacene Dimers. *Proc. Natl. Acad. Sci. U. S. A.* **2015**, *112*, 5325−5330.
(26) Eaton, S. W.; Shoer, L. E.; Karlen, S. D.; Dyar, S. M.; Margulies, E. A.; Veldkamp, B. S.; Ramanan, C.; Hartzler, D. A.; Savikhin, S.; Marks, T. J.; et al. Singlet Exciton Fission in Polycrystalline Thin Films of a Slip-Stacked Perylenediimide. *J. Am. Chem. Soc.* **2013**, *135*, 14701−14712.
(27) Wang, Z.; Zhao, J.; Barbon, A.; Toffoletti, A.; Liu, Y.; An, Y.; Xu, L.; Karatay, A.; Yaglioglu, H. G.; Yildiz, E. A.; et al. Radical-Enhanced Intersystem Crossing in New Bodipy Derivatives and Application for Efficient Triplet-Triplet Annihilation Upconversion. *J. Am. Chem. Soc.* **2017**, *139*, 7831−7842.
(28) Zhao, J.; Wu, W.; Sun, J.; Guo, S. Triplet Photosensitizers: From Molecular Design to Applications. *Chem. Soc. Rev.* **2013**, *42*, 5323−5351.
(29) Likhtenstein, G. I.; Ishii, K.; Nakatsuji, S. Dual Chromophore-Nitroxides: Novel Molecular Probes, Photochemical and Photophysical Models and Magnetic Materials. *Photochem. Photobiol.* **2007**, *83*, 871−881.
(30) Huang, Y.; Egap, E. Open-Shell Organic Semiconductors: An Emerging Class of Materials with Novel Properties. *Polym. J.* **2018**, *50*, 603−614.
(31) Green, S. A.; Simpson, D. J.; Zhou, G.; Ho, P. S.; Blough, N. V. Intramolecular Quenching of Excited Singlet States by Stable Nitroxyl Radicals. *J. Am. Chem. Soc.* **1990**, *112*, 7337−7346.
(32) Mizuochi, N.; Ohba, Y.; Yamauchi, S. First Observation of the Photoexcited Quintet State in Fullerene Linked with Two Nitroxide Radicals. *J. Phys. Chem. A* **1999**, *103*, 7749−7752.
(33) Franco, L.; Mazzoni, M.; Corvaja, C.; Gubskaya, V. P.; Berezhnaya, L. S.; Nuretdinov, I. A. First Observation of the Hyperfine Structure of an Excited Quintet State in Liquid Solution. *Chem. Commun.* **2005**, *33*, 2128−2130.
(34) Conti, F.; Corvaja, C.; Toffoletti, A.; Mizuochi, N.; Ohba, Y.; Yamauchi, S.; Maggini, M. EPR Studies on a Binitroxide Fullerene Derivative in the Ground Triplet and First Photoexcited Quintet State. *J. Phys. Chem. A* **2000**, *104*, 4962−4967.
(35) Teki, Y.; Miyamoto, S.; Nakatsuji, M.; Miura, Y. π-Topology and Spin Alignment Utilizing the Excited Molecular Field: Observation of the Excited High-Spin Quartet (S = 3/2) and Quintet (S = 2) States on Purely Organic π-Conjugated Spin Systems. *J. Am. Chem. Soc.* **2001**, *123*, 294−305.
(36) Takeuchi, S.; Ishii, K.; Kobayashi, N. Time-Resolved EPR and Transient Absorption Studies on Phthalocyaninatosilicon Covalently Linked to Two PROXYL Radicals. *J. Phys. Chem. A* **2004**, *108*, 3276−3280.
(37) Ratera, I.; Veciana, J. Playing with Organic Radicals as Building Blocks for Functional Molecular Materials. *Chem. Soc. Rev.* **2012**, *41*, 303−349.
(38) Nakatsuji, S. Recent Progress toward the Exploitation of Organic Radical Compounds with Photo-Responsive Magnetic Properties. *Chem. Soc. Rev.* **2004**, *33*, 348−353.
(39) Blättler, C.; Jent, F.; Paul, H. A Novel Radical-Triplet Pair Mechanism for Chemically Induced Electron Polarization (CIDEP) of Free Radicals in Solution. *Chem. Phys. Lett.* **1990**, *166*, 375−380.
(40) Kawai, A.; Okutsu, T.; Obi, K. Spin Polarization Generated in the Triplet-Doublet Interaction: Hyperfine-Dependent Chemically Induced Dynamic Electron Polarization. *J. Phys. Chem.* **1991**, *95*, 9130−9134.
(41) Kawai, A.; Obi, K. First Observation of a Radical-Triplet Pair Mechanism (RTPM) with Doublet Precursor. *J. Phys. Chem.* **1992**, *96*, 52−56.
(42) Nishide, H.; Nambo, M.; Miyasaka, M. Hyperbranched Poly(Phenylenevinylene) Bearing Pendant Phenoxys for a High-Spin Alignment. *J. Mater. Chem.* **2002**, *12*, 3578−3584.
(43) Nishide, H.; Miyasaka, M.; Doi, R.; Araki, T. Poly(1,2-Phenylenevinylene) Ferromagnetically 3,5-Bearing Phenoxyl Radicals. *Macromolecules* **2002**, *35*, 690−698.
(44) Nishide, H.; Kaneko, T.; Nii, T.; Katoh, K.; Tsuchida, E.; Yamaguchi, K. Through-Bond and Long-Range Ferromagnetic Spin Alignment in a.Pi.-Conjugated Polyradical with a Poly-(Phenylenevinylene) Skeleton. *J. Am. Chem. Soc.* **1995**, *117*, 548−549.
(45) Hayashi, H.; Yamamoto, T. Synthesis of Regioregular π-Conjugated Poly(Thienyleneethynylene) with a Hindered Phenolic Substituent. *Macromolecules* **1997**, *30*, 330−332.
(46) Miyasaka, M.; Yamazaki, T.; Tsuchida, E.; Nishide, H. Regioregular Polythiophene with Pendant Phenoxyl Radicals: A New High-Spin Organic Polymer. *Macromolecules* **2000**, *33*, 8211−8217.
(47) Levanon, H.; Norris, J. R. The Photoexcited Triplet State and Photosynthesis. *Chem. Rev.* **1978**, *78*, 185−198.
(48) Green, J. A.; Singer, L. A.; Parks, J. H. Fluorescence Quenching by the Stable Free Radical Di-t-Butylnitroxide. *J. Chem. Phys.* **1973**, *58*, 2690−2695.
(49) Chattopadhyay, S. K.; Das, P. K.; Hug, G. L. Photoprocesses in Diphenylpolyenes. 2. Excited-State Interactions with Stable Free Radicals. *J. Am. Chem. Soc.* **1983**, *105*, 6205−6210.

DOI: 10.1021/acs.chemmater.8b03366
Chem. Mater. 2018, 30, 7840−7851

(50) Samanta, A.; Kamat, P. V. Quenching of Fullerene Triplets by Stable Nitroxide Radicals. *Chem. Phys. Lett.* **1992**, *199*, 635−639.
(51) Araki, Y.; Luo, H.; Islam, S. D.-M.; Ito, O.; Matsushita, M. M.; Iyoda, T. Photoinduced Electron Transfer from Nitoxide Free Radicals to the Triplet State of C_{60}. *J. Phys. Chem. A* **2003**, *107*, 2815−2820.
(52) Schmidt, D.; Son, M.; Lim, J. M.; Lin, M.-J.; Krummenacher, I.; Braunschweig, H.; Kim, D.; Würthner, F. Perylene Bisimide Radicals and Biradicals: Synthesis and Molecular Properties. *Angew. Chem., Int. Ed.* **2015**, *54*, 13980−13984.
(53) Chernick, E. T.; Mi, Q.; Kelley, R. F.; Weiss, E. A.; Jones, B. A.; Marks, T. J.; Ratner, M. A.; Wasielewski, M. R. Electron Donor−Bridge−Acceptor Molecules with Bridging Nitronyl Nitroxide Radicals: Influence of a Third Spin on Charge- and Spin-Transfer Dynamics. *J. Am. Chem. Soc.* **2006**, *128*, 4356−4364.
(54) Colvin, M. T.; Carmieli, R.; Miura, T.; Richert, S.; Gardner, D. M.; Smeigh, A. L.; Dyar, S. M.; Conron, S. M.; Ratner, M. A.; Wasielewski, M. R. Electron Spin Polarization Transfer from Photogenerated Spin-Correlated Radical Pairs to a Stable Radical Observer Spin. *J. Phys. Chem. A* **2013**, *117*, 5314−5325.
(55) Dyar, S. M.; Margulies, E. A.; Horwitz, N. E.; Brown, K. E.; Krzyaniak, M. D.; Wasielewski, M. R. Photogenerated Quartet State Formation in a Compact Ring-Fused Perylene-Nitroxide. *J. Phys. Chem. B* **2015**, *119*, 13560−13569.
(56) Horwitz, N. E.; Phelan, B. T.; Nelson, J. N.; Krzyaniak, M. D.; Wasielewski, M. R. Picosecond Control of Photogenerated Radical Pair Lifetimes Using a Stable Third Radical. *J. Phys. Chem. A* **2016**, *120*, 2841−2853.
(57) Rugg, B. K.; Phelan, B. T.; Horwitz, N. E.; Young, R. M.; Krzyaniak, M. D.; Ratner, M. A.; Wasielewski, M. R. Spin-Selective Photoreduction of a Stable Radical within a Covalent Donor−Acceptor−Radical Triad. *J. Am. Chem. Soc.* **2017**, *139*, 15660−15663.
(58) Li, F.; Gore, D. N.; Wang, S.; Lutkenhaus, J. L. Unusual Internal Electron Transfer in Conjugated Radical Polymers. *Angew. Chem., Int. Ed.* **2017**, *56*, 9856−9859.
(59) Kawanaka, Y.; Shimizu, A.; Shinada, T.; Tanaka, R.; Teki, Y. Using Stable Radicals To Protect Pentacene Derivatives from Photodegradation. *Angew. Chem., Int. Ed.* **2013**, *52*, 6643−6647.
(60) Herbelin, S. E.; Blough, N. V. Intramolecular Quenching of Excited Singlet States in a Series of Fluorescamine-Derivatized Nitroxides. *J. Phys. Chem. B* **1998**, *102*, 8170−8176.
(61) Yee, W. A.; Kuzmin, V. A.; Kliger, D. S.; Hammond, G. S.; Twarowski, A. J. Quenching of the Fluorescent State of Rubrene Directly to the Ground State. *J. Am. Chem. Soc.* **1979**, *101*, 5104−5106.
(62) Ito, A.; Shimizu, A.; Kishida, N.; Kawanaka, Y.; Kosumi, D.; Hashimoto, H.; Teki, Y. Excited-State Dynamics of Pentacene Derivatives with Stable Radical Substituents. *Angew. Chem., Int. Ed.* **2014**, *53*, 6715−6719.
(63) Fujisawa, J.; Ishii, K.; Ohba, Y.; Yamauchi, S.; Fuhs, M.; Möbius, K. X- and W-Band Time-Resolved Electron Paramagnetic Resonance Studies on Radical-Excited Triplet Pairs between Metalloporphyrins and Axial-Ligating Nitroxide Radicals. *J. Phys. Chem. A* **1997**, *101*, 5869−5876.
(64) Fujisawa, J.; Ishii, K.; Ohba, Y.; Yamauchi, S.; Fuhs, M.; Möbius, K. First Observation of the Excited Doublet State of a Radical−Triplet Pair in Solution: W-Band High-Field Time-Resolved Electron Paramagnetic Resonance Spectroscopy. *J. Phys. Chem. A* **1999**, *103*, 213−216.
(65) Corvaja, C.; Maggini, M.; Prato, M.; Scorrano, G.; Venzin, M. C60 Derivative Covalently Linked to a Nitroxide Radical: Time-Resolved EPR Evidence of Electron Spin Polarization by Intramolecular Radical-Triplet Pair Interaction. *J. Am. Chem. Soc.* **1995**, *117*, 8857−8858.
(66) Giacobbe, E. M.; Mi, Q.; Colvin, M. T.; Cohen, B.; Ramanan, C.; Scott, A. M.; Yeganeh, S.; Marks, T. J.; Ratner, M. A.; Wasielewski, M. R. Ultrafast Intersystem Crossing and Spin Dynamics of Photoexcited Perylene-3,4:9,10-Bis(Dicarboximide) Covalently Linked to a Nitroxide Radical at Fixed Distances. *J. Am. Chem. Soc.* **2009**, *131*, 3700−3712.
(67) Colvin, M. T.; Giacobbe, E. M.; Cohen, B.; Miura, T.; Scott, A. M.; Wasielewski, M. R. Competitive Electron Transfer and Enhanced Intersystem Crossing in Photoexcited Covalent TEMPO−Perylene-3,4:9,10-Bis(Dicarboximide) Dyads: Unusual Spin Polarization Resulting from the Radical−Triplet Interaction. *J. Phys. Chem. A* **2010**, *114*, 1741−1748.
(68) Ishii, K.; Hirose, Y.; Kobayashi, N. Selective Population from the Excited Multiplet States to the Triplet Ground State in a Phthalocyanine: A New Concept for Controlling Magnetic Properties by Photoexcitation. *J. Am. Chem. Soc.* **1998**, *120*, 10551−10552.
(69) Ishii, K.; Fujisawa, J.; Adachi, A.; Yamauchi, S.; Kobayashi, N. General Simulations of Excited Quartet Spectra with Electron-Spin Polarizations: The Excited Multiplet States of (Tetraphenylporphinato)Zinc(II) Coordinated by p- or m-Pyridyl Nitronyl Nitroxides. *J. Am. Chem. Soc.* **1998**, *120*, 3152−3158.
(70) Xu, K.; Sukhanov, A. A.; Zhao, Y.; Zhao, J.; Ji, W.; Peng, X.; Escudero, D.; Jacquemin, D.; Voronkova, V. K. Unexpected Nucleophilic Substitution Reaction of BODIPY: Preparation of the BODIPY-TEMPO Triad Showing Radical-Enhanced Intersystem Crossing. *Eur. J. Org. Chem.* **2018**, *2018*, 885−895.
(71) Miura, Y.; Ushitani, Y.; Inui, K.; Teki, Y.; Takui, T.; Itoh, K. Syntheses and Magnetic Characterization of Poly(1,3-Phenyleneethynylene) with Pendant Nitronyl Nitroxide Radicals. *Macromolecules* **1993**, *26*, 3698−3701.
(72) Chernick, E. T.; Casillas, R.; Zirzlmeier, J.; Gardner, D. M.; Gruber, M.; Kropp, H.; Meyer, K.; Wasielewski, M. R.; Guldi, D. M.; Tykwinski, R. R. Pentacene Appended to a TEMPO Stable Free Radical: The Effect of Magnetic Exchange Coupling on Photoexcited Pentacene. *J. Am. Chem. Soc.* **2015**, *137*, 857−863.
(73) Roncali, J. Synthetic Principles for Bandgap Control in Linear π-Conjugated Systems. *Chem. Rev.* **1997**, *97*, 173−206.
(74) Chang, M.; Su, Z.; Egap, E. Alignment and Charge Transport of One-Dimensional Conjugated Polymer Nanowires in Insulating Polymer Blends. *Macromolecules* **2016**, *49*, 9449−9456.
(75) Chang, M.; Choi, D.; Egap, E. Macroscopic Alignment of One-Dimensional Conjugated Polymer Nanocrystallites for High-Mobility Organic Field-Effect Transistors. *ACS Appl. Mater. Interfaces* **2016**, *8*, 13484−13491.
(76) Mishra, A.; Ma, C.-Q.; Bäuerle, P. Functional Oligothiophenes: Molecular Design for Multidimensional Nanoarchitectures and Their Applications. *Chem. Rev.* **2009**, *109*, 1141−1276.
(77) Becker, R. S.; Seixas de Melo, J.; Maçanita, A. L.; Elisei, F. Comprehensive Evaluation of the Absorption, Photophysical, Energy Transfer, Structural, and Theoretical Properties of α-Oligothiophenes with One to Seven Rings. *J. Phys. Chem.* **1996**, *100*, 18683−18695.
(78) Becker, R. S.; de Melo, J. S.; Macanita, A. L.; Elisei, F. Comprehensive Investigation of the Solution Photophysics and Theoretical Aspects of Oligothiophenes of 1−7 Rings. *Pure Appl. Chem.* **1995**, *67*, 9−16.
(79) Nakazaki, J.; Chung, I.; Watanabe, R.; Ishitsuka, T.; Kawada, Y.; Matsushita, M. M.; Sugawara, T. Design of Spin-Polarized Molecular Wire as a Prototypal Unimolecular Quantum Spin Device. *Internet Electron. J. Mol. Des.* **2003**, *2*, 112−127.
(80) Eaton, S. S.; More, K. M.; Sawant, B. M.; Eaton, G. R. Use of the ESR Half-Field Transition to Determine the Interspin Distance and the Orientation of the Interspin Vector in Systems with Two Unpaired Electrons. *J. Am. Chem. Soc.* **1983**, *105*, 6560−6567.
(81) Zoppellaro, G.; Geies, A.; Andersson, K. K.; Enkelmann, V.; Baumgarten, M. Synthesis, Optical Properties and Magnetic Studies of 2,6-Bis(Pyrazolylmethyl)Pyridine Functionalized with Two Nitronyl Nitroxide Radicals. *Eur. J. Org. Chem.* **2008**, *2008*, 1431−1440.
(82) Mitsumori, T.; Inoue, K.; Koga, N.; Iwamura, H. Exchange Interactions between Two Nitronyl Nitroxide or Iminyl Nitroxide Radicals Attached to Thiophene and 2,2'-Bithienyl Rings. *J. Am. Chem. Soc.* **1995**, *117*, 2467−2478.
(83) Ullman, E. F.; Osiecki, J. H.; Boocock, D. G. B.; Darcy, R. Stable Free Radicals. X. Nitronyl Nitroxide Monoradicals and

DOI: 10.1021/acs.chemmater.8b03366
Chem. Mater. 2018, 30, 7840−7851

Biradicals as Possible Small Molecule Spin Labels. *J. Am. Chem. Soc.* **1972**, *94*, 7049−7059.
(84) Beljonne, D.; Cornil, J.; Friend, R. H.; Janssen, R. A. J.; Brédas, J. L. Influence of Chain Length and Derivatization on the Lowest Singlet and Triplet States and Intersystem Crossing in Oligothiophenes. *J. Am. Chem. Soc.* **1996**, *118*, 6453−6461.
(85) Beljonne, D.; Shuai, Z.; Pourtois, G.; Bredas, J. L. Spin−Orbit Coupling and Intersystem Crossing in Conjugated Polymers: A Configuration Interaction Description. *J. Phys. Chem. A* **2001**, *105*, 3899−3907.
(86) Li, C.; Evangelista, F. A. Multireference Driven Similarity Renormalization Group: A Second-Order Perturbative Analysis. *J. Chem. Theory Comput.* **2015**, *11*, 2097−2108.
(87) Hannon, K. P.; Li, C.; Evangelista, F. A. An Integral-Factorized Implementation of the Driven Similarity Renormalization Group Second-Order Multireference Perturbation Theory. *J. Chem. Phys.* **2016**, *144*, 204111.
(88) Becke, A. D. Density-functional Thermochemistry. III. The Role of Exact Exchange. *J. Chem. Phys.* **1993**, *98*, 5648−5652.
(89) Lee, C.; Yang, W.; Parr, R. G. Development of the Colle-Salvetti Correlation-Energy Formula into a Functional of the Electron Density. *Phys. Rev. B: Condens. Matter Mater. Phys.* **1988**, *37*, 785−789.
(90) Weigend, F.; Ahlrichs, R. Balanced Basis Sets of Split Valence, Triple Zeta Valence and Quadruple Zeta Valence Quality for H to Rn: Design and Assessment of Accuracy. *Phys. Chem. Chem. Phys.* **2005**, *7*, 3297−3305.
(91) Matsuda, K.; Matsuo, M.; Irie, M. Photoswitching of Intramolecular Magnetic Interaction Using Diarylethene with Oligothiophene π-Conjugated Chain. *J. Org. Chem.* **2001**, *66*, 8799−8803.
(92) Fazzi, D.; Canesi, E. V.; Negri, F.; Bertarelli, C.; Castiglioni, C. Biradicaloid Character of Thiophene-Based Heterophenoquinones: The Role of Electron-Phonon Coupling. *ChemPhysChem* **2010**, *11*, 3685−3695.
(93) Nishizawa, S.; Hasegawa, J.; Matsuda, K. Theoretical Investigation on the Decaying Behavior of Exchange Interaction in Quinoid and Aromatic Molecular Wires. *J. Phys. Chem. C* **2015**, *119*, 5117−5121.
(94) Kasha, M. Characterization of Electronic Transitions in Complex Molecules. *Discuss. Faraday Soc.* **1950**, *9*, 14−19.
(95) Suppan, P. *Chemistry and Light*; Royal Society of Chemistry, 1994.
(96) Lakowicz, J. R. *Principles of Fluorescence Spectroscopy*; Springer US: Boston, MA, 2006.
(97) Weller, A. Photoinduced Electron Transfer in Solution: Exciplex and Radical Ion Pair Formation Free Enthalpies and Their Solvent Dependence. *Z. Phys. Chem.* **1982**, *133*, 93−98.
(98) Matsumoto, K.; Fujitsuka, M.; Sato, T.; Onodera, S.; Ito, O. Photoinduced Electron Transfer from Oligothiophenes/Polythiophene to Fullerenes (C_{60} /C_{70}) in Solution: Comprehensive Study by Nanosecond Laser Flash Photolysis Method. *J. Phys. Chem. B* **2000**, *104*, 11632−11638.

DOI: 10.1021/acs.chemmater.8b03366
Chem. Mater. 2018, 30, 7840−7851